NOTICE CONCERNING COPYRIGHT RESTRICTIONS

Seismic While Drilling for Geophysical Exploration in a Geothermal Well

Flavio Poletto[1], Piero Corubolo[1], Andrea Schleifer[1], Biancamaria Farina[1], Joseph S. Pollard[2], and Brad Grozdanich[2]

[1]OGS Istituto Nazionale di Oceanografia e di Geofisica Sperimentale, Trieste, Italy
[2]DHI Services Inc., Texas, USA

Keywords

Geophysics, borehole, seismic, while drilling, imaging

ABSTRACT

We present the results of a seismic-while-drilling (SWD) survey performed using the working drill-bit as a seismic source in a Geothermal well in the U.S. (Gabbs Valley, NV). The SWD method was tuned and adapted for geothermal exploration purposes, to provide while-drilling and after-drilling geophysical results. These consist of the while-drilling prediction of obstacles and structural variations ahead of the bit by means of single-offset vertical seismic profiles (VSP) and multi-offset VSP. They also include interpretation of selected diffractions as related to faults, and the imaging of the well area by SWD data migration. The SWD results are compared to the other well information, and are in agreement with the drilling and interpreted geological data.

Introduction

Seismic while drilling (SWD) using the drill-bit noise is a known borehole-seismic technology developed and used to support drilling of Oil & Gas exploration wells from a geophysical point of view (Rector and Marion, 1991; Poletto and Miranda, 2004). The technology and method used in this experiment is a geothermal-adapted application of the Seisbit® SWD technology using the drill-bit source to provide while-drilling reverse vertical seismic profile (RVSP) for oil exploration purposes (Poletto and Miranda, 2004). The geothermal SWD survey was conducted in a well drilled in the Gabbs Valley (NV), part of a trans-tensional area characterised by the presence of major NW trending strike slip faults leading to very complex patterns and structures on the small scale (Faulds et al., 2005). The well was drilled close to a NE striking normal fault connecting the right-lateral faults, as hydrothermal fluids up-flow may occur at locations associated with fractures and fault intersections.

The purpose of this work was to provide while-drilling geophysical information ahead and around the bit, to obtain information about main fault location, and provide imaging of the surrounding structural geological setting in the well area characterized by complex structural conditions. In this paper we present a summary of the SWD geothermal application and while-drilling geophysical results, interpreted together with the drilling results.

Drill-Bit SWD Concept

To perform the SWD geothermal application we used only surface measurements of the drill-bit signals. The drill-bit SWD basic concept by only surface recordings is summarized in Fig. 1. The drill-bit signal propagates through the formations from the bit to the ground surface, where it is recorded by geophones, and propagates through the drill pipes to the top of the drill string,

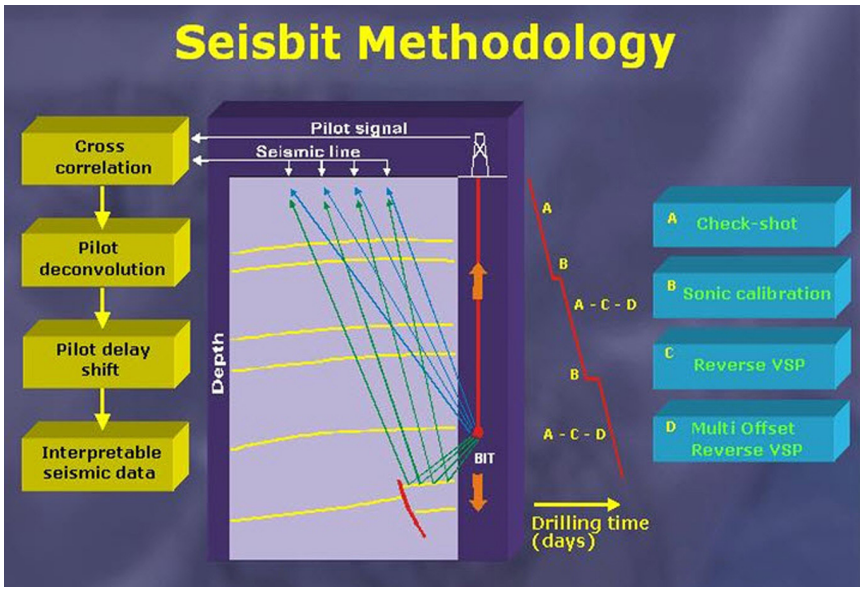

Figure 1. Basic concept of the seismic-while-drilling drill-bit method.

where it is recorded by reference (pilot) sensors. After signal cross-correlation, deconvolution and time correction to compensate for the pilot delay, one obtains interpretable seismograms, which provide while-drilling RVSP. The application has important advantages for geothermal wells, as it does not require downhole instrumentation, which may be sensitive to high temperature, and provides at nearly the same cost of near-offset recordings a set of multi-offset data useful for investigations extended around the well, which is even more important in complex fractured zones.

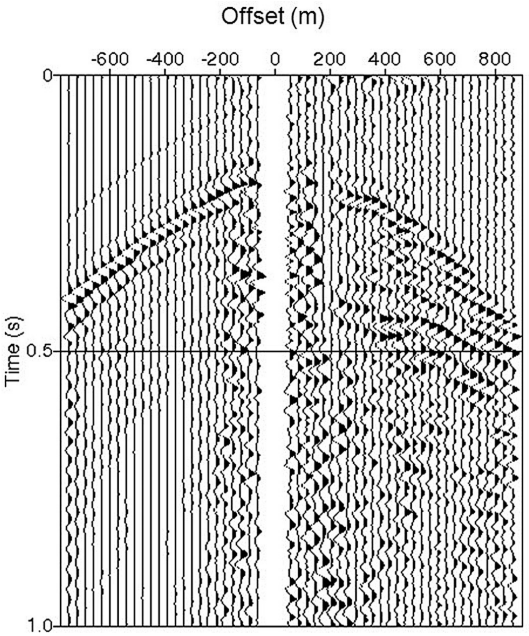

Figure 3. Example of L4-L2 SWD shot at drill-bit depth 440 m. The well position is at 0 m offset.

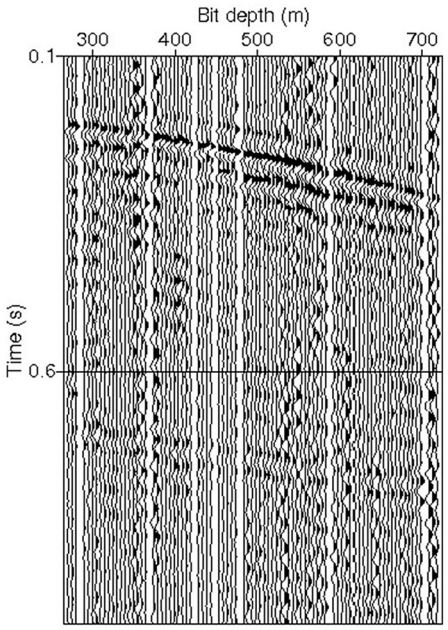

Figure 4. Example of SWD RVSP data (total wavefield).

Acquisition Layout

The pre-drilling geological information was derived mainly from gravity and magneto-telluric profiles. The gravity model was converted into a initial seismic model used to design the layout of the surface seismic lines, with two principal lines of surface geophones oriented in the (expected) direction perpendicular to the main fault system (line branches L2 and L4 in Fig. 2), and a cross-control seismic line (line branches L3 and L1 in Fig. 2) oriented in a nearly perpendicular direction to monitor possible lateral effects. The seismic lines were composed of traces recorded by receiver arrays of vertical geophones, spaced with inter-trace distance of 30 m. A lower number of horizontal geophones was used at control positions to monitor shear wavefields. The lines L4 and L2 were designed with offset ranging from -750 m to 870 m from wellhead, respectively, taking into account the expected wavefields:

- L4, for the detection of reflections from the expected silicified fault-zone reflections, and
- L2, to obtain information about observable diffraction events above the main fault zone.

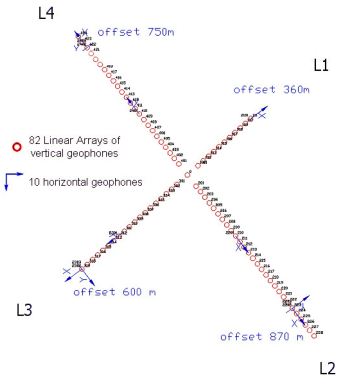

Figure 2. Layout of the SWD seismic line. Inter-trace distance between vertical geophone groups is 30 m.

Survey Acquisition

Automated SWD data acquisition was performed with continuous monitoring of the mud-logging drilling parameters. The survey started at drilling depth of approximately 180 m and was performed down to 750 m drilling depth. Acquisition levels were sampled in depth by collecting source shots on average every 5 m bit-depth interval. The SWD data were pre-processed in the field with the near-real-time remote quality control support from OGS headquarters, where the geophysical information was processed and interpreted while drilling for seismic data analysis and characterization of the drilled well area .

Figure 3 shows an example of L4-L2 field shot data obtained with the drill-bit source at 440 m depth. We can observe appreciable differences in signals along the left side (negative-offset L4) and right side (positive-offset L2) seismic lines, due to the different subsurface structural settings. In particular, events with the trend of diffraction hyperbola can be interpreted at intermediate position offset (450 m) along L2 and at time of approximately 0.5 s. Figure 4 shows an example of field SWD reverse VSP data recorded at a fixed-offset trace of the line L4 with different bit-source depths. These data are equivalent to conventional wire-line and used as a reverse VSP.

SWD Results

The SWD RVSP data were used for standard while-drilling reflection-ahead monitoring, and for diffraction-event interpretation. They were further processed for imaging by signal travel-time and waveform analysis, and by tomographic inversion (Böhm et al., 2005) to build the geological model and to perform data migration.

Prediction Results

Prediction ahead of the bit was obtained by interpreting the reflection signals, obtained after direct-arrival picking of the total SWD RVSP wavefields (see for example the total field of Fig. 4) and up-going wavefield separation.

Figure 5 shows examples of while-drilling prediction of formations ahead of the bit by single-offset SWD RVSP of selected traces of (5a) lines L3 and (5b) L4, respectively. Figures 5a and 5b represent the two-way-time (TWT) deconvolved up-going

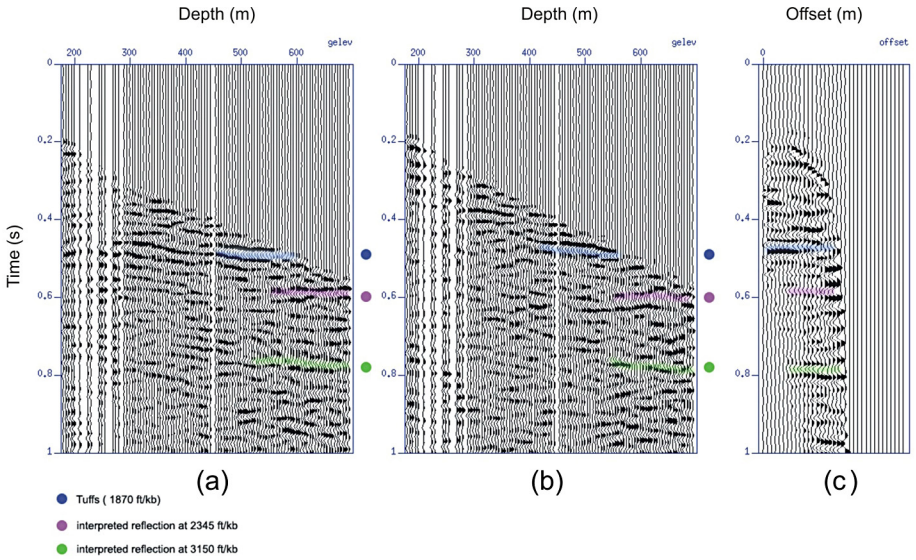

Figure 5. SWD prediction ahead of the bit by (a) and (b) single-offset RVSP, and (c) multi-offset RVSP. Bullets represent interpreted reflections at main formation changes. The reflection at approximately 0.5 s correlates well with the encountered alluvium/ash-tuff boundary, while the reflection at 0.6 s is interpreted as correlated to a lost-circulation zone inside the tuff.

wavefields, where the interpreted formation changes are marked by bullets. Figure 5c shows the interpretation of the corresponding events in a multi-offset SWD RVSP of line L2.

Imaging Results

The analysis of the direct arrivals in the SWD RVSP signals was extended to all the traces of the surfaces seismic lines, to obtain depth seismic images along the principal lines L4 and L2. The picked arrival times were analyzed to design the seismic model in the well area: using step-by-step stripped analysis of travel-time curves vs. offset obtained with the bit source at different depth levels, and supported by tomographic inversion of the measured travel-times (Böhm et al, 2005).

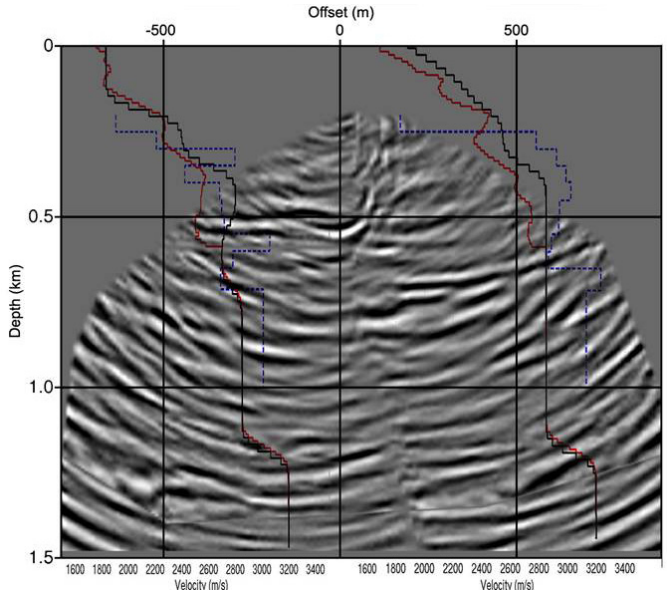

Figure 6. SWD L4-L2 data migration and SWD RVSP velocity profiles. The well location is at offset 0 m. Superimposed, seismic VSP velocity.

The seismic velocity model built and updated while drilling was used to migrate in depth the SWD up-going reflection data, using the compressional signal component, after wavefield separation and mitigation of the converted wave components. Figure 6 shows the SWD depth migration results and the SWD RVSP seismic velocity curves at different positions along lines L4 (negative offset) and line L2 (positive offset).

The 2D migration was calculated with 10 m and 5 m grid intervals, and variable aperture angles, to mitigate lateral artefacts at large offsets, and, at the same time, to include the expected reflection events due to the fault system in the silicified zone located in the proximity of the well below line L2.

The 2D depth migration model was used to extend the investigation laterally with respect to the well, and to further analyze the signals by support of full waveform analysis (see next section).

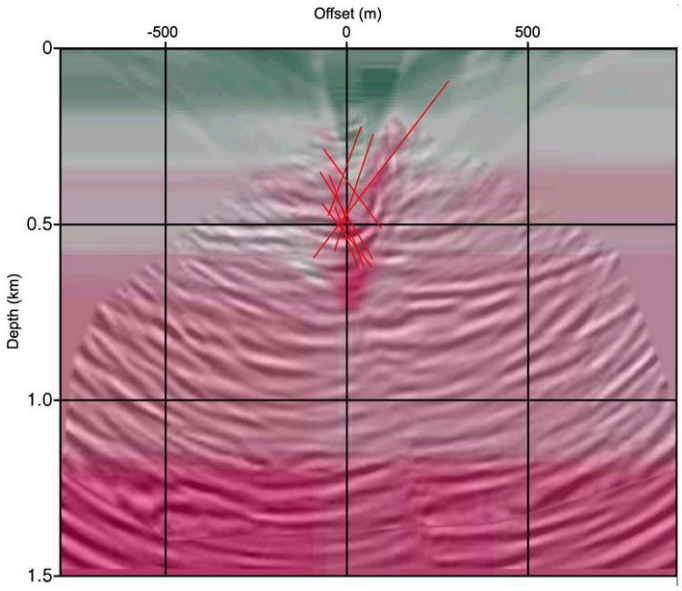

Figure 7. SWD L4-L2 data migration. The well location is at offset 0 m. Superimposed, tomography and fault system interpretation (by drilling information).

Figure 7 shows the direct-arrival tomographic velocity inversion superimposed to the SWD depth migration section. In the same figure, we plot the fault's interpretation based on the well results, logs and fracture-dip measurements. We can observe the matching of the depth migration imaging, of the tomographic velocity inversion at the well location, and of the interpreted fault system. In particular, a fault was encountered by drilling at about 460 m depth. This event was predicted by SWD data, and it is observable in the imaging migrated results.

The migration result is in agreement with the interpretation of the projected section of the shallow magneto-telluric anomaly (superimposed yellow spots) observable in the correspondence of

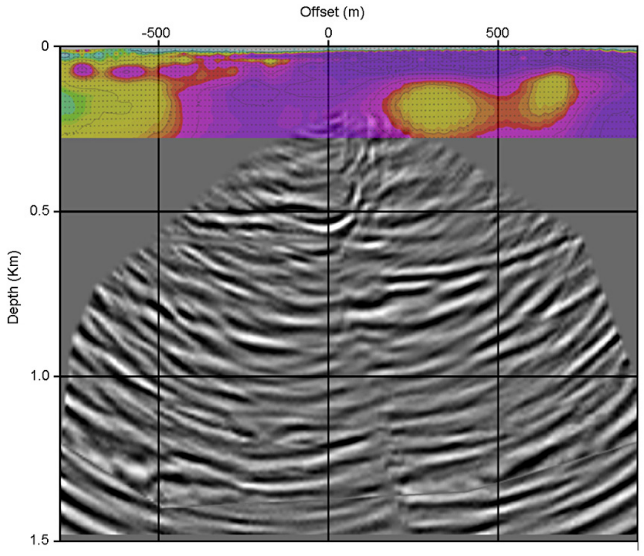

Figure 8. SWD L4-L2 data migration. The well location is at offset 0 m. Superimposed, the magneto-telluric results.

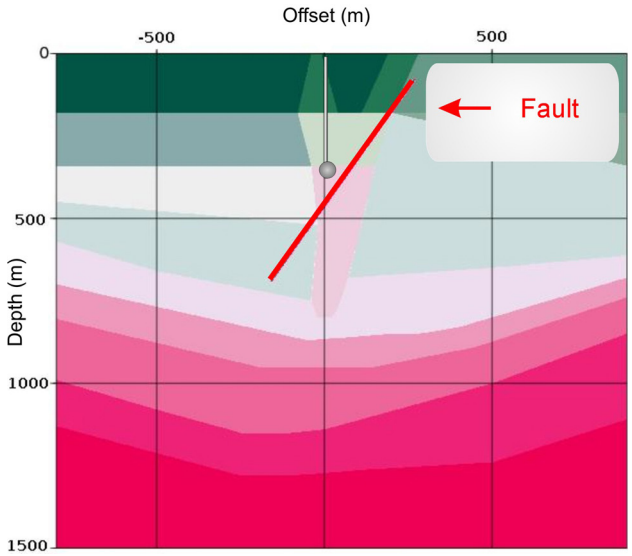

Figure 9. SWD L4-L2 seismic velocity model with a fault interpreted in the well results and in the results of Fig. 7.

the hot-water high-velocity intrusion zone (Fig. 8). In this shallow zone, the coverage by SWD reflections is absent because the survey started at depth 180 m, and because of the lateral position. In subsequent results, not presented in this work, we used the interferometry redatuming method to extend the SWD images at shallower depth and lateral offset (Poletto et al., 2011).

Fault Analysis

We integrate the imaging results with the analysis and the interpretation of the recorded SWD wavefields (full-waveform analysis). Based on the velocity and geological model obtained from travel-time inversion and 2D migration processing, assuming negligible lateral effects, we calculate synthetic signals corresponding to the real field shots, including structural discontinuities and fluid-filled faults (Wu et al., 2002; Gritto and Majer, 2002). We show an example of shot with the analysis of the main fault encountered by drilling along the well path, and with in-well measured 53 deg dip angle (Fig. 9, and also Fig. 7). To estimate the "fault response" we calculate the synthetic signals with fault and without fault, and subtract the results. Similar analysis shown here for the main fault was performed with other interpreted diffraction events.

To include the fluid-filled fault in the model we used a refined grid mesh. The SWD synthetic data were calculated with a 2D visco-elastic finite difference (FD) code. The numerical simulation model was discretized using a grid of 2500 × 2500 pixels, whose dimensions are $\Delta x = \Delta z = 1$ m. The normal thickness of the fluid-filled fault was 3 m. The vertical source was a Ricker wavelet with 30 Hz peak frequency, and the signal propagation was calculated for 1 s, with the output time-sampling rate of 1 ms. The seismic receivers were located at the ground-model surface,

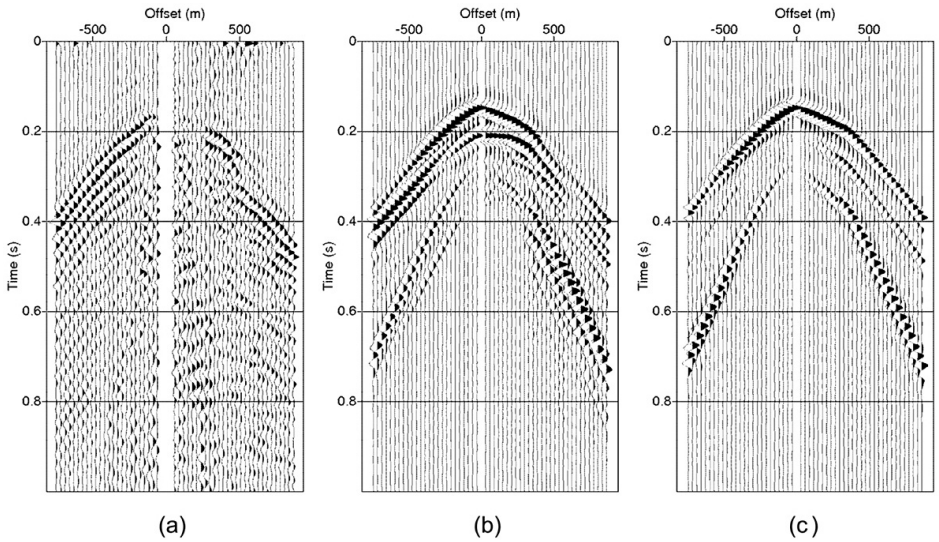

Figure 10. a) Signal of the real SWD shot compared to the corresponding synthetic signals calculated using the numerical model (b) with and (c) without fault.

with a the distance between each other of 1 m. The recorded signal were subsequently grouped and stacked to reproduce the 30-m arrays of the recording line.

Figure 10 shows the comparison of (10a) real SWD data recorded at bit depth 335 m and the synthetic signals obtained by the models (10b) with and (10c) without fluid-filled fault, respectively. Figure 11 compares again (11a) the SWD real data with (11b) the fault response calculated as the difference of the synthetic shots of Figs. 10b and 10c. The signal corresponding to the fault response can be clearly interpreted in the full-waveform real data (11a) at approximately 0.2 s and 200 m offset.

Discussion and Conclusions

In conclusion, good-quality data were acquired during a SWD survey in the US and results provided seismic information

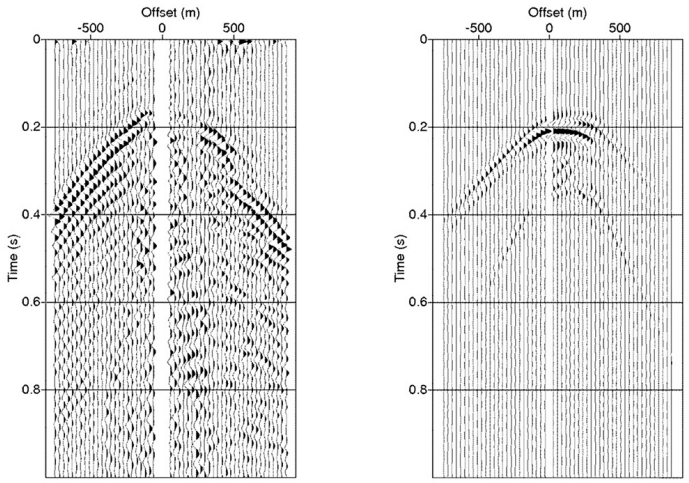

Figure 11. Synthetic fault-response (b) obtained by the difference of (10b) and (10c), compared to the corresponding real signal (a) where a fault diffraction can be clearly interpreted at approximately 0.2 s and 200 m offset.

ahead of the bit and around the geothermal well. The analysis shows that SWD prediction and imaging results are in agreement with the encountered well results and with the fault dip interpretation.

During this work we tuned the standard SWD procedure for the geothermal purposes. Important aspects emerged during the analysis are:

- Geothermal wells have good operational conditions for SWD application;
- SWD data can be used to provide the seismic information of the area in the absence of surface reflection seismic data;
- The SWD results can be integrated with other geological/geophysical information and with the drilling results to update while drilling the structural model;
- The imaging method integrated with the full-waveform analysis can be used while drilling for fault system characterization.

Acknowledgments

Authors would like to thank DHI for the technical support during SWD, and Gualtiero Böhm for his help in preparing the tomography inversion results.

References

Böhm G., I. Marson, L. Petronio, and F. Palmieri, 2005. "Integrated 3D inversion of seismic and gravimetric data on a real case." 75th Ann. Internat. Mtg: Soc. of Expl. Geophys.

Faulds J. E., C. D. Henry, and N. H. Hinz, 2005. "Kinematics of the northern Walker Lane: An incipient transform fault along the Pacific – North American plate boundary." Geology, v. 33, p. 505-508.

Gritto R., and E. L. Majer, 2002. "Seismic Methods for Resource Exploration in Enhanced Geothermal Systems." LBNL 52967.

Poletto F., and F. Miranda, 2004. "Seismic while drilling. Fundamentals of drill-bit seismics for exploration." Elsevier, Amsterdam.

Poletto F., P. Corubolo, B. Farina, A. Schleifer, J. Pollard, M. Peronio, and G. Böhm, 2011. "Drill-bit SWD and seismic interferometry for imaging around geothermal wells." Exp. Abst. SEG Conference San Antonio, in press.

Rector III J. W., and B. P. Marion, 1991. "The use of drill-bit energy as a downhole seismic source." Geophysics, v. 56, p. 628-634.

Wu C., J. M. Harris, and K. T. Nihei, 2002. "2D finite-difference seismic modeling for a single fluid-filled fracture: comparison of thin-layer and linear-slip models." 72n Ann. Internat. Mtg: Soc. of Expl. Geophys, pp. 1959-1962.